

# Electromagnetic form factors of light vector mesons

F.T. Hawes

*Department of Physics and Mathematical Physics,  
University of Adelaide, South Australia 5005, Australia*

M.A. Pichowsky

*Department of Physics and Supercomputer Computations Research Institute,  
Florida State University, Tallahassee, FL 32306-4130, USA  
(October 30, 2021)*

The electromagnetic form factors  $G_E(q^2)$ ,  $G_M(q^2)$ , and  $G_Q(q^2)$ , charge radii, magnetic and quadrupole moments, and decay widths of the light vector mesons  $\rho^+$ ,  $K^{*+}$  and  $K^{*0}$  are calculated in a Lorentz-covariant, Dyson-Schwinger equation based model using algebraic quark propagators that incorporate confinement, asymptotic freedom, and dynamical chiral symmetry breaking, and vector meson Bethe-Salpeter amplitudes closely related to the pseudoscalar amplitudes obtained from phenomenological studies of  $\pi$  and  $K$  mesons. Calculated static properties of vector mesons include the charge radii and magnetic moments:  $\langle r_{\rho^+}^2 \rangle^{1/2} = 0.61$  fm,  $\langle r_{K^{*+}}^2 \rangle^{1/2} = 0.54$  fm, and  $\langle r_{K^{*0}}^2 \rangle = -0.048$  fm<sup>2</sup>;  $\mu_{\rho^+} = 2.69$ ,  $\mu_{K^{*+}} = 2.37$ , and  $\mu_{K^{*0}} = -0.40$ . The calculated static limits of the  $\rho$ -meson form factors are similar to those obtained from light-front quantum mechanical calculations, but begin to differ above  $q^2 = 1$  GeV<sup>2</sup> due to the dynamical evolution of the quark propagators in our approach.

## I. INTRODUCTION

The electromagnetic (EM) form factors of hadrons provide an important tool for the study of bound states in QCD. There have been numerous experimental and theoretical studies of the  $\pi$ - and  $K$ -meson EM form factors  $F_\pi(q^2)$  and  $F_K(q^2)$  which have improved our understanding of the dynamics of quarks and gluons in hadrons [1–3]. Fewer studies have been undertaken for the three independent vector-meson EM form factors  $F_1(q^2)$ ,  $F_2(q^2)$  and  $F_3(q^2)$ , even though they would provide information about bound-state dynamics that is unobtainable from pseudoscalar-meson studies alone. In particular, EM gauge invariance constrains the *static limits* ( $q^2 = 0$ ) of  $F_\pi(q^2)$ ,  $F_K(q^2)$  and  $F_1(q^2)$  to equal the charge of the  $\pi$ ,  $K$  and vector mesons, respectively. Hence, the values of these form factors at  $q^2 = 0$  provide *no* dynamical information. The lack of such a constraint on  $F_2(q^2)$  and  $F_3(q^2)$  means that vector mesons have non-trivial static properties (their electric and magnetic moments). These provide information about bound-state dynamics in the limit that the vector meson does not recoil from the EM probe.

Light vector-meson EM form factors have received less attention than their pseudoscalar counterparts because their experimental determination is more difficult. The short lifetime of vector mesons (exemplified by the ratio of the  $K^{*-}$  and  $K$ -meson lifetimes,  $\tau_{K^*}/\tau_K \approx 10^{-14}$ ) has so far excluded the possibility of a direct measurement. However, indirect measurements of the static limits of the EM form factors are possible. For example, radiative decays of vector mesons, such as  $\rho^+ \rightarrow \pi^+\pi^0\gamma$ ,

may be used to obtain their magnetic moments [4], and charge radii may be inferred from the  $t$ -dependence of cross sections for diffractive vector-meson electroproduction. Such measurements are currently accessible at TJ-NAF, DESY, and FermiLab.

Herein, the EM form factors for  $\rho^+$ ,  $K^{*+}$  and  $K^{*0}$  mesons are calculated using model confined-quark propagators from Ref. [3] and vector-meson Bethe-Salpeter (BS) amplitudes that are a simple extension of the pseudoscalar BS amplitudes also developed in Ref. [3]. In the present study, the ramifications of employing vector-meson BS amplitudes that are closely related to their pseudoscalar counterparts are explored. The parameters introduced for the model  $\rho$ - and  $K^*$ -meson BS amplitudes are determined from a fit to the experimental values for the  $\rho^+ \rightarrow \gamma\pi^+$ ,  $\rho \rightarrow e^+e^-$ , and  $K^{*+} \rightarrow \gamma K^+$  decay widths. The calculated vector-meson EM form factors, associated moments and charge radii are then compared to those obtained by other theoretical studies [5,6]. The motivation of this study is to develop simple model BS amplitudes for light vector mesons and to provide experience and insight necessary for future studies of two- and three-body bound states. Such model amplitudes are important for a wide range of phenomenological applications including studies of effects outside the standard model [7], diffractive vector-meson electroproduction [8], and  $\rho$ - $\omega$  mixing [9].

## II. MODEL SCHWINGER FUNCTIONS

The use of model confined-quark propagators and meson BS amplitudes, based on studies of the Dyson-Schwinger equations of QCD, has proved efficacious to the study of hadron phenomena. The large number of observables correlated within the framework using only a few model Schwinger functions allows one to constrain the model forms of these functions. Such constraints make the framework highly predictive, which is tested in applications to processes outside the domain in which the model Schwinger functions were originally constrained. One example of this is found in Ref. [8], in which  $u$ -,  $d$ - and  $s$ -quark propagators and  $\pi$ - and  $K$ -meson BS amplitudes, developed in low-energy studies of  $\pi$  and  $K$  meson decays and EM form factors, were employed in a study of high-energy ( $\sqrt{s} \geq 10$  GeV)  $\pi$ -nucleon and  $K$ -nucleon diffractive scattering and Pomeron exchange.

In the following, the  $s$ -quark propgator parameters, originally obtained in Ref. [3], are recalculated by fitting to  $K$ -meson observables and quark condensates. This fitting procedure leads to an  $s$ -quark propagator and  $K$ -meson BS amplitude that is more consistent with recent numerical studies of the Bethe-Salpeter equation [10].

### A. Quark propagators and pseudoscalar BS amplitudes

Numerical studies [11] of the coupled, Dyson-Schwinger and Bethe-Salpeter equations in the  $u$ - and  $d$ -quark sectors obtain solutions similar in form to those developed in Ref. [3]. Recent and more extensive studies (which include the  $s$ -quark sector) [10] obtain  $K$ -meson BS amplitudes that are qualitatively different than the model forms developed in Ref. [3]. To improve the connection between the model Schwinger functions employed herein and the solutions obtained from numerical studies of the Dyson-Schwinger and Bethe-Salpeter equations, the  $s$ -quark propagator parameters are refitted to  $K$ -meson observables.

The new  $s$ -quark propagator is obtained by starting with the model  $u$ -quark propagator and then allowing only 2 of the parameters to vary from their  $u$ -quark values. The parameters are determined by fitting the  $K$ -meson weak decay constant  $f_K$  and mass  $m_K$ , and by demanding that the  $s$ -quark in-vacuum and  $s$ -quark in-kaon condensates and current  $s$ -quark mass  $m_s$  are the same as those obtained in Ref. [10]. The first application of the new  $s$ -quark parametrization is in a calculation of the charge radii of the neutral- and charged- $K$  mesons.

The form of the model dressed-quark propagators is based on numerical studies of the quark Dyson-Schwinger equation with a realistic model-gluon propagator [11]. In a general covariant gauge, the quark propagator is written as  $S_f(k) = -i\gamma \cdot k \sigma_V^f(k^2) + \sigma_S^f(k^2)$ , and is well-described by the following parametrization:

$f/\text{meson}$	$b_0^f$	$b_1^f$	$b_2^f$	$b_3^f$	$C^f$	$m_f$ [MeV]
$u, d$	0.131	2.900	0.603	0.185	0	5.1
$\pi$	same	same	same	same	0.121	0
$\rho$	0.044	0.580	same	0.462	0	0
$s$	0.105	2.900	0.540	0.185	0	130.0
$K$	0.322	same	same	same	0	0
$K^*$	0.107	0.870	same	0.092	0	0

TABLE I. Confined-quark propagator parameters for  $u$ ,  $d$ , and  $s$  quarks from Ref. [3]. An entry of “same” for a meson indicates that the value of the parameter is the same as for the quark flavor with which it is grouped.

$$\begin{aligned}\bar{\sigma}_S^f(x) &= \left(b_0^f + b_2^f \mathcal{F}[\epsilon x]\right) \mathcal{F}[b_1^f x] \mathcal{F}[b_3^f x] \\ &\quad + 2\bar{m}_f \mathcal{F}[2(x + \bar{m}_f^2)] + C_{m_f} e^{-2x}, \\ \bar{\sigma}_V^f(x) &= \frac{2(x + \bar{m}_f^2) - 1 + e^{-2(x + \bar{m}_f^2)}}{2(x + \bar{m}_f^2)^2},\end{aligned}\quad (2.1)$$

where

$$\mathcal{F}[x] = \frac{1 - e^{-x}}{x}, \quad (2.2)$$

with  $x = k^2/\lambda^2$ ,  $\bar{\sigma}_S^f = \lambda \sigma_S^f$ ,  $\bar{\sigma}_V^f = \lambda^2 \sigma_V^f$ ,  $\bar{m}_f = m_f/\lambda$ ,  $\lambda = 0.566$  GeV, and  $\epsilon = 10^{-4}$ . This dressed-quark propagator has *no* Lehmann representation and hence describes the propagation of a confined quark. It also reduces to a bare-fermion propagator when its momentum is large and spacelike, in accordance with the asymptotic behavior expected from perturbative QCD (up to logarithmic corrections).

The parameters for the  $u$ - and  $d$ -quark propagators are assumed to be the same ( $SU(2)$ -flavor symmetric). Their values were determined in Ref. [3] by performing a  $\chi^2$  fit to a range of  $\pi$ - and  $K$ -meson observables. The resulting parameters are given in Table I.

In the chiral limit ( $m_f = 0$ ), it follows from Goldstone’s theorem that the pseudoscalar-meson BS amplitude  $\Gamma_{\mathcal{P}}(k; p)$  is completely determined by the dressed quark propagator  $S_f(k)$  [10]. If the amplitude is taken to be proportional to lowest Dirac moment,  $\gamma_5$ , it is given by

$$\Gamma_{\mathcal{P}}(k; p) = \gamma_5 \frac{B_{\mathcal{P}}(k^2)}{f_{\mathcal{P}}} \quad (2.3)$$

for  $\mathcal{P} = \pi$ - or  $K$ -mesons, where  $B_{\mathcal{P}}(k^2)$  is the Lorentz-scalar function appearing in the quark inverse propagator  $S_f^{-1}(k) = i\gamma \cdot k A_f(k^2) + B_f(k^2)$ . Here,  $f_{\mathcal{P}}$  is the pseudoscalar-meson weak-decay constant and can be evaluated from the BS normalization\*:

\* A formulation of quantum field theory is employed using

$$f_P^2 = \frac{p_\mu}{p^2} N_c \text{tr} \int \frac{d^4 k}{(2\pi)^4} B_P^2(k^2) \times \left( \frac{d}{dp_\mu} S_s(k + \frac{1}{2}p) \gamma_5 S_u(k - \frac{1}{2}p) \gamma_5 + S_s(k + \frac{1}{2}p) \gamma_5 \frac{d}{dp_\mu} S_u(k - \frac{1}{2}p) \gamma_5 \right), \quad (2.4)$$

where  $S_f(k)$  is the propagator for a quark with flavor  $f$ ,  $B_P(k^2)$  is from the BS amplitude for the pseudoscalar,  $P = \pi$  or  $K$  meson in Eq. (2.3), with total momentum  $p$  and relative quark-antiquark momentum  $k$ ,  $N_c = 3$ , and  $\text{tr}$  denotes a trace over the Dirac indices.

Using the definition in Ref. [2], the in-vacuum quark condensate obtained from the model quark propagator of Eq. (2.1) is

$$\langle \bar{q}^f q^f \rangle_{\text{vac}}^\mu = -\lambda^3 \left( \ln \frac{\mu^2}{\Lambda_{\text{QCD}}^2} \right) \frac{3}{4\pi^2} \frac{b_0^f}{b_1^f b_3^f}. \quad (2.5)$$

The  $s$ -quark parameters are chosen as follows. The magnitude of the  $s$ -quark condensate in the vacuum is taken to be 80% that of the  $u$  quark. The scales  $b_1^f$  and  $b_3^f$  in Eq. (2.1) are flavor independent ( $b_1^s = b_1^u$  and  $b_3^s = b_3^u$ ) so that Eq. (2.5) fixes the value of  $b_0^s = 0.80 b_0^u$ . A relation for the “in-kaon” quark condensate  $\langle \bar{q}^s q^s \rangle_K^\mu$  is obtained from Eq. (2.5) with the replacement  $b_0^s \rightarrow b_0^K$ . The requirement that this condensate and the current-quark mass  $m_s$  have the same values as obtained in Ref. [10] at the renormalization point  $\mu = 1$  GeV, determines  $b_0^K = 3.07 b_0^s$ .

The  $K$ -meson mass  $m_K$  is determined from the relation:

$$f_K^2 m_K^2 = -\langle \bar{q}^s q^s \rangle_{\mu^2}^K (m_u + m_s). \quad (2.6)$$

The value of  $b_2^s$  is obtained by performing a  $\chi^2$  fit to the experimental values of  $f_K$  and  $m_K$ . The resulting parameters are given in Table I, the resulting weak decay width,  $K$ -meson mass and  $s$ -quark condensates are given in Table II.

The first application that will serve as a test of the new parametrization of the  $s$ -quark propagator is a calculation of the charged and neutral  $K$ -meson charge radii. The charge radius is related to the  $K$ -meson EM form factor by

$$\langle r_{K^+}^2 \rangle = -6 \lim_{q^2 \rightarrow 0} \frac{d}{dq^2} F_{K^+}(q^2), \quad (2.7)$$

and  $F_{K^+}(q^2)$  is obtained from the  $\gamma K^+ K^-$  vertex:

the Euclidean metric  $\delta_{\mu\nu} = \text{diag}(1, 1, 1, 1)$  with the convention that spacelike momentum  $q_\mu$  satisfies  $q^2 = q \cdot q = q_\mu q_\mu > 0$ , and Dirac matrices  $\gamma_\mu$  that satisfy:  $\gamma_\mu^\dagger = \gamma_\mu$  and  $\{\gamma_\mu, \gamma_\nu\} = 2\delta_{\mu\nu}$ .

	this study	experiment
$f_K$	0.112	$0.113 \pm 0.001$
$m_K$	0.491	$0.494 \pm 0.016$
$-\langle \bar{q}^s q^s \rangle_0^{1/3}$	0.198	$0.175 - 0.205$
$-\langle \bar{q}^s q^s \rangle_K^{1/3}$	0.289	—
$\langle r_{K^+}^2 \rangle^{1/2}$	0.528	$0.582 \pm 0.041$
$\langle r_{K^0}^2 \rangle$	-0.032	$-0.054 \pm 0.026$

TABLE II. Calculated  $K$ -meson observables and  $s$ -quark condensates evaluated at  $\mu = 1$  GeV. All values are given in units of GeV, except  $\langle r_{K^+}^2 \rangle^{1/2}$  is in fm, and  $\langle r_{K^0}^2 \rangle$  is in  $\text{fm}^2$  [1]. Experimental values given for condensates are those obtained from theoretical studies (see Ref. [3]).

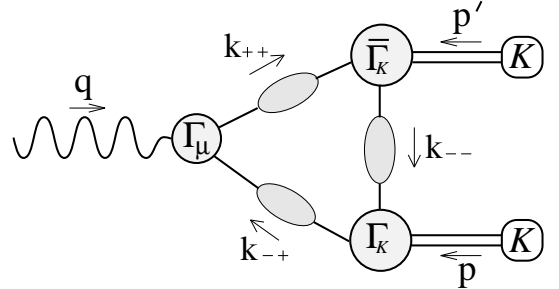


FIG. 1. One contribution to the proper  $\gamma K \bar{K}$  vertex.

$$\Lambda_\mu^{K^+}(p, p') = \frac{1}{2}(p - p')_\mu F_{K^+}(q^2) + \frac{1}{2}(p + p')_\mu G_{K^+}(q^2), \quad (2.8)$$

where  $p$  ( $p'$ ) is the four-momentum of the initial (final)  $K$  meson,  $q = -p - p'$  is the four-momentum of the photon. In this elastic ( $p^2 = p'^2$ ) process, the form factors depend only on  $q^2$  and  $G_K(q^2) = 0$  for all  $q^2$ . In the impulse approximation, the  $\gamma K^+ K^-$  vertex is given by:

$$\Lambda_\mu^{K^+}(p, p') = \frac{2}{3} \Lambda_\mu^{u\bar{s}}(p, p') + \frac{1}{3} \Lambda_\mu^{\bar{s}u}(p, p'), \quad (2.9)$$

with

$$\Lambda_\mu^{u\bar{s}}(p, p') = 2N_c \text{tr} \int \frac{d^4 k}{(2\pi)^4} S_u(k_{++}) i\Gamma_\mu(k_{++}, k_{-+}) \times S_u(k_{-+}) \bar{\Gamma}_K(k - \frac{1}{2}q; -p') \times S_s(k_{--}) \Gamma_K(k; p), \quad (2.10)$$

$$\Lambda_\mu^{\bar{s}u}(p, p') = 2N_c \text{tr} \int \frac{d^4 k}{(2\pi)^4} S_s(k_{++}) i\Gamma_\mu(k_{++}, k_{-+}) \times S_s(k_{-+}) \Gamma_K(k - \frac{1}{2}q; -p') \times S_u(k_{--}) \bar{\Gamma}_K(k; p), \quad (2.11)$$

where  $k_{ab} = k + \frac{a}{2}q + \frac{b}{2}p$ ,  $N_c = 3$ ,  $\Gamma_K(k; p)$  is the pseudoscalar  $K$ -meson BS amplitude,  $\Gamma_\mu(k, k')$  is the dressed quark-photon vertex,  $S_f(k)$  is the dressed propagator for a confined-quark of flavor  $f$  and “tr” denotes a trace over Dirac indices. The adjoint pseudoscalar-meson BS amplitude is given by  $\bar{\Gamma}_K(k; -p) = C^T \Gamma_K^T(-k; -p) C$ , where

$C = \gamma_2 \gamma_4$  and  $T$  denotes the transpose of Dirac indices. The proper  $\gamma K^0 \bar{K}^0$  vertex is given by Eqs. (2.9)–(2.11) with the relabeling  $u \rightarrow d$  and the replacement of the coefficient  $\frac{2}{3}$  by  $-\frac{1}{3}$  in Eq. (2.9). For comparison, the proper  $\gamma \pi^+ \pi^-$  vertex would be given by Eqs. (2.9)–(2.11) with the relabeling  $K \rightarrow \pi$  and  $s \rightarrow d$ . The diagram corresponding to Eq. (2.10) or (2.11) is shown in Fig. 1.

Evaluation of the EM form factors from Eqs. (2.9)–(2.11) requires an explicit form for the quark-photon vertex  $\Gamma_\mu(k, k')$ . The quark-photon vertex  $\Gamma_\mu(k, k')$  transforms under charge conjugation, space and time inversion in a manner similar to the bare vertex  $\gamma_\mu$  and must satisfy the Ward-Takahashi identity (WTI). The most general quark-photon vertex, free of kinematic singularities, that fulfills these requirements is written as  $\Gamma_\mu^T(k, k') + \Gamma_\mu^{BC}(k, k')$  [12], where  $\Gamma_\mu^T(k, k')$  is transverse to the photon momentum  $q_\mu = (k - k')_\mu$  and  $\Gamma_\mu^{BC}(k, k')$ , determined from the WTI, is [13]:

$$i\Gamma_\mu^{BC}(k, k') = \frac{i}{2}\gamma_\mu f_1 + \frac{i}{2}(k + k')_\mu \gamma \cdot (k + k') f_2 + (k + k')_\mu f_3, \quad (2.12)$$

with  $f_1 = A_f(k^2) + A_f(k'^2)$ ,  $f_2 = (A_f(k^2) - A_f(k'^2))/(k^2 - k'^2)$ ,  $f_3 = (B_f(k^2) - B_f(k'^2))/(k^2 - k'^2)$ , where  $A_f(k^2)$  and  $B_f(k^2)$  are the Lorentz invariant functions in the dressed-quark inverse propagator  $S_f^{-1}(k) = i\gamma \cdot k A_f(k^2) + B_f(k^2)$ . The addition of transverse contributions to the quark-photon vertex in  $\Gamma_\mu^T(k, k')$  are unimportant for the calculation of observables at space-like momenta [14]; they vanish as both  $k^2$  and  $k'^2$  become large and spacelike in accordance with the asymptotic freedom of QCD and vanish in the limit that  $k - k' \rightarrow 0$  by the Ward identity. In the following, these transverse contributions are neglected and the dressed quark-photon vertex is taken to be  $\Gamma_\mu^{BC}(k, k')$ .

Calculating the quark-loop integration in Eqs. (2.10) and (2.11), one obtains the  $K$ -meson EM form factors and associated charge radii. Their values are given in Table II.

## B. Vector meson BS amplitudes

The model vector-meson BS amplitudes, to be used in Sec. III to calculate the EM form factors of the  $\rho^+$ ,  $K^{*+}$  and  $K^{*0}$  vector mesons, are similar to the pseudoscalar amplitudes discussed above. The Ansatz for the vector-meson BS amplitude  $V_\mu(k; p)$  is

$$V_\mu(k; p) = \mathbf{T}_{\mu\nu}(p) \gamma_\nu \frac{B_V(k^2)}{N_V}, \quad (2.13)$$

where  $\mathbf{T}_{\mu\nu}(p) = \delta_{\mu\nu} + p_\mu p_\nu / M^2$  and  $M$  is the mass of the vector meson  $V$ . The BS normalization  $N_V$  is obtained from the BS normalization equation, which is a simple generalization of Eq. (2.4).

The difference between the pseudoscalar- and vector-meson BS amplitudes is provided for by allowing  $b_0^\mathcal{V}$ ,  $b_1^\mathcal{V}$

and  $b_3^\mathcal{V}$  to differ from the values  $b_0^\rho$ ,  $b_1^\rho$  and  $b_3^\rho$ . This simple Ansatz supplies a minimal difference that is sufficient for the purposes of this present study of the low- $q^2$  behavior of the EM form factors. For large values of  $q^2$ , one expects that other Dirac structures, not included in Eq. (2.13), may be important. This is indeed what is observed in studies of pseudoscalar mesons, where the term proportional to  $\gamma_5 \gamma \cdot p$  ( $p$  is the total momentum of the pseudoscalar bound state) must be included in the BS amplitude to reproduce the correct, asymptotic- $q^2$  behavior of the form factor [16]. Higher Dirac moments may also be important for the calculation of some hadronic decays. For example, in quark-model calculations, the particular choice of quantum numbers for the  $q\bar{q}$  interaction which induces the  $\rho \rightarrow \pi\pi$  decay has a considerable impact on the coupling constant  $g_{\rho\pi\pi}$  [17]. In particular, this decay is better described within quantum mechanics in terms of an interaction that has  $^{2s+1}L_J = ^3P_0$  quantum numbers, rather than  $^3S_1$ . The latter being equivalent to a one-gluon-exchange interaction. Such sensitivity to the quantum numbers could show up in the present, covariant model, as an enhancement of higher Dirac moments.

Using the simple Ansatz given by Eq. (2.13), it is impossible to obtain simultaneous agreement with the experimental decay widths for  $\rho \rightarrow \pi\pi$ ,  $\rho \rightarrow e^+e^-$  and  $\rho \rightarrow \gamma\pi$  for any reasonable<sup>†</sup> choice of parameters. On the other hand, one may obtain a satisfactory fit by relaxing the constraint of reproducing the experimental decay width for  $\rho \rightarrow \pi\pi$ . This may, in fact, support the notion that this process is particularly sensitive to higher-order Dirac structures in the BS amplitude which have been neglected in Eq. (2.13). However, a complete study of the importance of higher Dirac moments would require a careful analysis of the vector-meson BS equation, its dependence on the 8 possible Dirac structures present in the full vector-meson BS amplitude, and the extent to which higher Dirac moments affect vector-meson observables. The present investigation of vector-meson EM form factors is a necessary prerequisite of such a study.

The magnitude of  $b_0^\rho$  is closely related to the  $\rho$ -meson EM charge radius and should take a value  $0 \leq b_0^\rho \leq b_0^\pi$  to ensure the phenomenologically desirable result:  $\langle r_\rho^2 \rangle \leq \langle r_\pi^2 \rangle$ . On this domain, varying the value of  $b_0^\rho$  affects the  $\rho$ -meson charge radius by less than 10% and the median value of  $\langle r_\rho^2 \rangle$  occurs when  $b_0^\rho \approx \frac{1}{3}b_0^\pi$ . The constraint  $b_0^\mathcal{V} = \frac{1}{3}b_0^\rho$ , where  $\mathcal{V} = \rho$  ( $K^*$ ) and  $\mathcal{P} = \pi$  ( $K$ ), is employed here, as a means to minimize the number of free parameters in Eq. (2.13). The remaining parameters,  $b_1^\rho$  and  $b_3^\rho$  are then obtained from a  $\chi^2$  fit to the decay constants:  $f_\rho$  and  $g_{\rho\pi\pi}$ , and  $b_1^{K^*}$  and  $b_3^{K^*}$  are fit to  $g_{\gamma K^* K}$ . The resulting

<sup>†</sup> The parameters are chosen so that the resulting vector BS amplitudes are monotonic functions of  $k^2$ , as observed in numerical studies.

parameters are summarized in Table I and the calculated decay constants and their experimental values are given in Table III.

The formulae necessary to calculate  $\rho^+ \rightarrow \gamma\pi^+$  are described in Ref. [18], while those necessary to calculate  $\rho^0 \rightarrow e^+e^-$  and  $\rho \rightarrow \pi\pi$  are discussed in Ref. [8]. The decay constant  $g_{\gamma K^*K}$  for the  $K^* \rightarrow \gamma K$  decay is obtained from an obvious generalization of the definition for  $g_{\gamma\rho\pi}$  in Ref. [18], with the observation that isospin invariance requires:

$$\Gamma_{K^{*+} \rightarrow K^+\pi^0} = \frac{1}{3}\Gamma_{K^{*+} \rightarrow K\pi} \approx 16.6 \pm 0.3 \text{ MeV}. \quad (2.14)$$

The experimental value of the coupling constant calculated from Eq. (2.14) is  $g_{K^*K\pi} = 6.40 \pm 0.06$ .

### III. ELECTROMAGNETIC FORM FACTORS OF VECTOR MESONS

The EM current of a vector meson is

$$\langle -p' \lambda' | J_\mu(q) | p \lambda \rangle = \Lambda_{\mu\alpha\beta}(p, p') \varepsilon_\alpha(p, \lambda) \varepsilon_\beta^*(-p', \lambda'), \quad (3.1)$$

where  $q = -p' - p$  is the photon momentum and  $\varepsilon_\alpha(p, \lambda)$  is the polarization vector of a vector meson with helicity  $\lambda$ . Bose symmetry and charge conjugation require that the proper vertex satisfies  $\Lambda_{\mu\alpha\beta}(p, p') = -\Lambda_{\mu\beta\alpha}(p', p)$  so that the most general Lorentz covariant form of  $\Lambda_{\mu\alpha\beta}(p, p')$  is

$$\Lambda_{\mu\alpha\beta}(p, p') = -\sum_{j=1}^3 T_{\mu\alpha\beta}^{[j]}(p, p') F_j(q^2), \quad (3.2)$$

where

$$\begin{aligned} T_{\mu\alpha\beta}^{[1]}(p, p') &= (p_\mu - p'_\mu) \mathbf{T}_{\alpha\gamma}(p) \mathbf{T}_{\gamma\beta}(p'), \\ T_{\mu\alpha\beta}^{[2]}(p, p') &= \mathbf{T}_{\mu\alpha}(p) \mathbf{T}_{\beta\delta}(p') p_\delta - \mathbf{T}_{\mu\beta}(p') \mathbf{T}_{\alpha\delta}(p) p'_\delta, \\ T_{\mu\alpha\beta}^{[3]}(p, p') &= \frac{1}{2M^2} (p_\mu - p'_\mu) \mathbf{T}_{\alpha\gamma}(p) p'_\gamma \mathbf{T}_{\beta\delta}(p') p_\delta, \end{aligned} \quad (3.3)$$

and  $\mathbf{T}_{\mu\nu}(p)$  is defined below Eq. (2.13). An alternative set of tensors whose vector-meson Lorentz indices transform irreducibly under spatial rotations in the Breit frame may be constructed from linear combinations of these [15]. The form factors associated with this set of *irreducible tensors* are the electric-monopole, magnetic-dipole and electric-quadrupole form factors,  $G_E$ ,  $G_M$ , and  $G_Q$ , respectively, and in our notation, they are related to  $F_1$ ,  $F_2$ , and  $F_3$  according to

$$\begin{aligned} G_E &= F_1 + \frac{2}{3} \frac{q^2}{4M^2} G_Q, \\ G_M &= -F_2, \\ G_Q &= F_1 + F_2 + (1 + \frac{q^2}{4M^2}) F_3. \end{aligned} \quad (3.4)$$

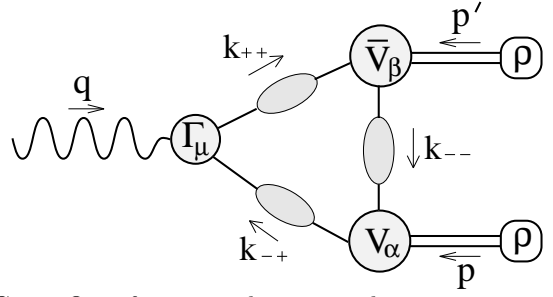


FIG. 2. One of two contributions to the proper  $\gamma\rho\rho$  vertex.

#### A. Impulse approximation

In impulse approximation, the proper  $\gamma K^{*+} K^{*-}$  vertex is given by

$$\Lambda_{\mu\alpha\beta}^{K^{*+}}(p, p') = \frac{2}{3} \Lambda_{\mu\alpha\beta}^{u\bar{s}}(p, p') + \frac{1}{3} \Lambda_{\mu\alpha\beta}^{\bar{s}u}(p, p'), \quad (3.5)$$

with

$$\begin{aligned} \Lambda_{\mu\alpha\beta}^{u\bar{s}}(p, p') &= 2N_c \text{tr} \int \frac{d^4k}{(2\pi)^4} S_u(k_{++}) i\Gamma_\mu(k_{++}, k_{-+}) \\ &\quad \times S_u(k_{-+}) \bar{V}_\beta(k - \eta_+ q; -p') \\ &\quad \times S_s(k_{--}) V_\alpha(k; p), \end{aligned} \quad (3.6)$$

$$\begin{aligned} \Lambda_{\mu\alpha\beta}^{\bar{s}u}(p, p') &= 2N_c \text{tr} \int \frac{d^4k}{(2\pi)^4} S_s(k_{++}) i\Gamma_\mu(k_{++}, k_{-+}) \\ &\quad \times S_s(k_{-+}) V_\alpha(k - \eta_- q; -p') \\ &\quad \times S_u(k_{--}) \bar{V}_\beta(k; p), \end{aligned} \quad (3.7)$$

where  $k_{ab} = k + a\eta_+ q + b\eta_- p$  in Eq. (3.6),  $k_{ab} = k + a\eta_- q + b\eta_+ p$  in Eq. (3.7),  $\eta_+ + \eta_- = 1$ ,  $\eta_+$  is the fraction of total bound-state momentum carried by the  $u$  quark, and  $V_\alpha(k; p)$  is the vector-meson BS amplitude. The adjoint vector-meson BS amplitude is given by  $\bar{V}_\alpha(k; -p) = C^T V_\alpha^T(-k; -p) C$ , where  $C = \gamma_2 \gamma_4$  and  $T$  denotes the transpose of Dirac indices. The proper  $\gamma\rho^+\rho^-$  vertex is given by Eqs. (3.5)–(3.7) with the relabeling  $s \rightarrow d$  and the proper  $\gamma K^{*0} \bar{K}^{*0}$  vertex is given by Eqs. (3.5)–(3.7) with the relabeling  $u \rightarrow d$  and the replacement of the coefficient  $\frac{2}{3}$  by  $-\frac{1}{3}$  in Eq. (3.5). The diagram corresponding to Eqs. (3.6) and (3.7) is shown in Fig. 2.

#### B. Numerical results

Having determined the parameters in the vector-meson BS amplitude, one may calculate the EM form factors directly from Eqs. (3.6) and (3.7). The resulting form factors are shown in Figs. 3 – 5.

The nodal structures of the form factors are typical of spin-1 systems.  $F_1(q^2)$  has a node at moderate  $q^2$ ,  $F_3(q^2)$  has a node at a higher  $q^2$  and  $F_2(q^2)$  has no nodes. From the relations in Eqs. (3.4), one finds that  $G_E(q^2)$  has then two nodes,  $G_Q(q^2)$  has one node and  $G_M(q^2)$  has

	this study	rel. QM [6]	experiment
$f_\rho$	4.37		$5.05 \pm 0.12$
$g_{\gamma\rho\pi}$	0.62		$0.57 \pm 0.03$
$g_{\gamma K^* K}$	0.98		$0.75 \pm 0.03$
$g_{\rho\pi\pi}$	8.52		$6.03 \pm 0.02$
$g_{K^* K\pi}$	9.66		$6.40 \pm 0.04$
$\langle r_{\rho^+}^2 \rangle^{1/2}$	0.61 fm	$0.61 \pm 0.014$ fm	$(\sim 0.61$ fm)
$\langle r_{K^{*+}}^2 \rangle^{1/2}$	0.54 fm		
$\langle r_{K^{*0}}^2 \rangle$	-0.048 fm <sup>2</sup>		
$\mu_{\rho^+}$	2.69	$2.23 \pm 0.13$	
$\mu_{K^{*+}}$	2.37		
$\mu_{K^{*0}}$	-0.40		
$\bar{Q}_{\rho^+}$	$0.055$ fm <sup>2</sup>	$0.048 \pm 0.012$ fm <sup>2</sup>	
$\bar{Q}_{K^{*+}}$	$0.029$ fm <sup>2</sup>		
$\bar{Q}_{K^{*0}}$	$-0.0049$ fm <sup>2</sup>		

TABLE III. Calculated vector meson observables. The quoted magnetic moments are the dimensionless values  $G_M(0)$  where  $\mu = G_M(0)\frac{e\hbar}{2M}$ , quadrupole moments are  $\bar{Q} = -G_Q(0)\frac{1}{M^2}$  where  $M$  is the mass of the vector meson. The “experimental” value of  $\langle r_{\rho^+}^2 \rangle^{1/2}$  is estimated from diffractive electroproduction data [21] and results from relativistic quantum mechanics are provided [6].

none. The node in  $G_Q(q^2)$  and second node in  $G_E(q^2)$  occur above  $q^2 = 10$  GeV<sup>2</sup> hence they are not depicted in Figs. 3 – 5. The location of the first node in  $G_E(q^2)$  gives a measure of the size of the vector meson. Its appearance at a smaller  $q^2$  for the  $\rho^+$  meson relative to that of the  $K^{*+}$  is indicative of the larger size of the  $\rho^+$ .

The canonical measure of the size of a bound state is the charge radius, defined in Eq. (2.7). The charge radius of the  $\rho^+$  meson has also been calculated within relativistic quantum mechanical models [5,6]. The mean charge radius obtained from and the deviation between these models is  $\langle r_{\rho^+}^2 \rangle^{1/2} = 0.61 \pm 0.014$  fm. The result of the present model is  $\langle r_{\rho^+}^2 \rangle^{1/2} = 0.61$  fm.

It is important to note that the charge radii that result from our calculations of Eqs. (3.6) and (3.7) represent only the contributions due to the quark-antiquark substructure of the vector meson. Additional contributions arising from meson loops may be present but have been neglected in this study and in Refs. [5,6]. In the case of the pion form factor, the effect of including  $\pi$ -meson loops is minimal, tending to increase the pion charge radius by less than 15% [19]. However, meson loops have a qualitatively different effect on the vector-meson form factors. The light vector mesons are massive enough to decay into two pseudoscalars. Therefore, two-pseudoscalar meson loops in vector-meson self-energies give rise to nonanalyticities associated with this decay. Such nonanalyticities may have significant impact on certain observables, particularly the charge radii of *neutral* particles. An example of this is the semileptonic decays  $K \rightarrow \pi\ell\nu_\ell$  and

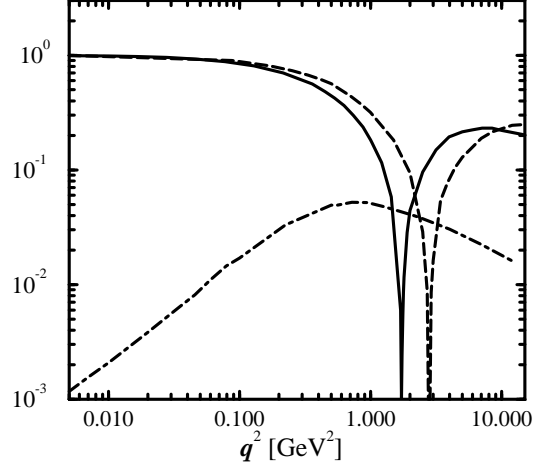


FIG. 3. The electric-monopole form factor  $|G_E(q^2)|$  for  $\rho^+$  (solid),  $K^{*+}$  (dashed) and  $K^{*0}$  (dot-dashed) mesons. The sign of  $G_E(0)$  is positive for each of the mesons considered.

$\pi \rightarrow \pi\ell\nu_\ell$ . It was shown that subthreshold  $K\pi$  loops contribute significantly to the quark-antiquark- $W$ -boson vertex for *timelike*  $W$ -boson momenta [20]. The most significant effect on an observable being an increase in obtained radius for the  $\pi$ - $K$  transition form factor by up to 50%. Nonetheless, since such contributions fall off rapidly with increasing spacelike momenta, they are expected to have a smaller effect on the *spacelike* EM form factors considered here. The role and importance of pion loops in determining the  $\rho$ -meson EM form factors for timelike and spacelike photon momenta requires further investigation.

Although a direct measurement of the  $\rho$ -meson charge radius is not possible at present, there is an empirical relation between the  $t$  dependence of diffractive  $\rho$ -meson electroproduction and a “diffractive radius” of the vector meson. The “diffractive radius” that is inferred from electroproduction data is  $r_\rho \approx 0.61$  fm [21]. However, the agreement between the “diffractive radius” and the charge radii obtained in Refs. [5,6] and herein should be viewed with caution since the relationship between these quantities is not understood.

It is apparent from Figs. 3 – 5 that the neutral  $K^*$  meson form factor is not identically zero for all  $q^2$ . In general, the EM form factors of charge-conjugate non-identical, neutral mesons (such as the  $K^{*0}$  and  $\bar{K}^{*0}$  mesons) will not be identically zero for all  $q^2$ . This results from the breakdown of SU(3)-flavor symmetry caused by the mass difference between the  $u$  and  $s$  quarks. The negative value of  $\langle r_{K^{*0}}^2 \rangle$  is indicative of the larger mass of the  $s$  quark. Of course, the EM form factors for the neutral- $\rho$  meson are absent from the present study because the assumption of exact isospin invariance at the level of the quark dynamics (i.e.,  $S_u(k) = S_d(k)$ ) entails that they are identically zero for all  $q^2$ .

Of course, the value of  $G_E(q^2)$  at  $q^2 = 0$  is propor-

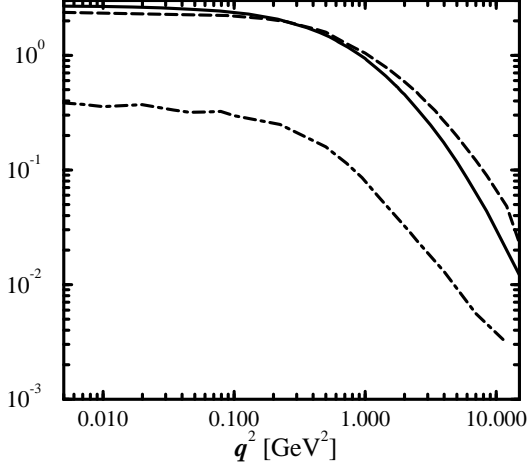


FIG. 4. The magnetic-dipole form factor  $|G_M(q^2)|$  for  $\rho^+$  (solid),  $K^{*+}$  (dashed) and  $K^{*0}$  (dot-dashed) mesons. The sign of  $G_M(0)$  is positive for  $\rho^+$  and  $K^{*+}$  and negative for  $K^{*0}$ .

tional to the EM charge of the vector meson. In the numerical calculation of a neutral meson form factor, a result of  $G_E(0) \neq 0$  would be indicative of a violation of charge conservation in Eqs. (3.6) and (3.7). In the present study, charge conservation (i.e.,  $G_E^{K^{*0}}(0) = 0$ ) is ensured in Eqs. (3.6) and (3.7), with the assumption that the  $u$  quark carries a fraction  $\eta_+ = 0.45$  of the total bound-state momentum  $p$  while the  $\bar{s}$  quark carries the fraction  $1 - \eta_+$ . Had the assumption of equal partitioning ( $\eta_+ = 1/2$ ) been made, a small violation to charge conservation would have ensued. This violation would have been  $G_E(0) = 0.0032$ .

It was shown in Ref. [10], that charge conservation is maintained within the impulse approximation through the use of BS amplitudes, satisfying the Bethe-Salpeter equation, in which the full dependence on the invariant  $k \cdot p$  is maintained. (Here,  $k$  is the relative quark-antiquark momentum and  $p$  is the total bound state momentum.) In this study, we have employed simplified model BS amplitudes, having only the dominant Lorentz structure  $\mathbf{T}_{\mu\nu}(p)\gamma_\nu$  and arguments that are  $O(4)$  symmetric; i.e., independent of  $k \cdot p$ . Therefore, charge conservation was ensured through the choice of  $\eta_+ = 0.45$  in Eqs. (3.6) and (3.7).

Overall, the agreement between the  $\rho$ -meson form factors obtained from our model and those obtained from relativistic quantum mechanical models is quite good for small  $q^2$ . Below  $q^2 = 1 \text{ GeV}^2$ , both approaches are expected to be reliable and the agreement achieved may be indicative of this. For example, the mean charge radius and quadrupole moment obtained in Ref. [6] is  $\langle r_\rho^2 \rangle^{1/2} = 0.61 \pm 0.014 \text{ fm}$  and  $\bar{Q} = 0.048 \pm 0.012 \text{ fm}^2$  while those obtained in the present study are  $\langle r_\rho^2 \rangle^{1/2} = 0.61 \text{ fm}$  and  $\bar{Q} = 0.055 \text{ fm}^2$ , respectively. However, the discrepancy between the magnetic-dipole moment obtained in Ref. [6]

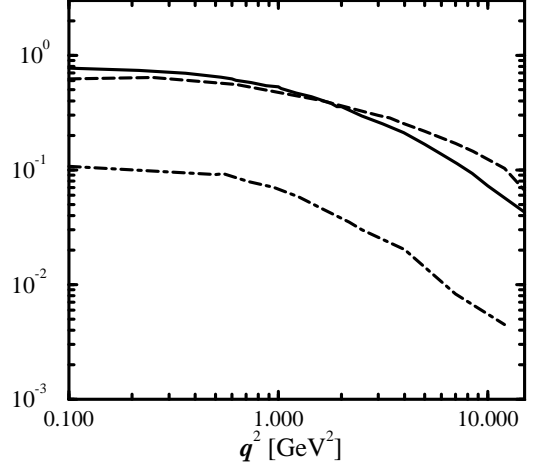


FIG. 5. The electric-quadrupole form factor  $|G_Q(q^2)|$  for  $\rho^+$  (solid),  $K^{*+}$  (dashed) and  $K^{*0}$  (dot-dashed) mesons. The sign of  $G_Q(0)$  is negative for  $\rho^+$  and  $K^{*+}$  and positive for  $K^{*0}$ .

$\mu = 2.23 \pm 0.13 [e_0/2M_\rho]$ , and that obtained in the present study  $\mu = 2.69 [e_0/2M_\rho]$  is significant. An experimental determination of vector-meson magnetic moments provides a tool with which to probe the various model frameworks.

Furthermore, in the present study, a close relation between the charge radius and magnetic moment of a vector meson and the infrared behavior of its BS amplitude is observed. A measurement of either of these observables would provide information about the infrared behavior of the vector-meson BS amplitudes. Such information is important, as it provides crucial constraints on future numerical studies of vector-meson bound states in QCD.

An important difference between quantum mechanical models and Dyson-Schwinger-based models is that quantum mechanical models typically employ a constituent quark with a mass  $M_\rho/2$ , while in our approach, quarks are confined and have *no* mass pole at all. The mass-scales in the quark propagator  $S_f(k)$  of Eq. (2.1) evolve dynamically with the quark momentum, being constituent-like near  $k^2 = 0$  and becoming current-like as  $k^2 \rightarrow \infty$ . Therefore, at low- $q^2$ , one expects the two approaches to produce similar results, and (with the exception of the magnetic moment) the results obtained herein are in complete agreement with those of Ref. [6].

However, above  $q^2 = 1 \text{ GeV}^2$  the results of relativistic quantum mechanics begin to differ from those calculated herein. For example, the location of the first node in  $G_E(q^2)$ , as obtained in Refs. [5,6], occurs at  $q^2 \approx 3 \text{ GeV}^2$ , while it is found from our calculation to be near  $1.73 \text{ GeV}^2$ . This discrepancy results from two differences between quantum mechanical models and our Dyson-Schwinger based model. The first is the use of *dynamical* mass-scales in the quark propagator  $S_f(k)$  from Eq. (2.1), as discussed above. The transition in the

quark propagator  $S_f(k)$  from a constituent-like quark to a current-like quark becomes important in the calculation of EM form factors for photon momenta greater than  $q^2 \approx 1 \text{ GeV}^2$ . This feature is common to processes involving photo-meson transitions and has been observed in studies of diffractive electroproduction of vector mesons [8] and the  $\gamma^* \pi \rightarrow \gamma$  transition form factor [22]. The second difference is the sensitivity of the vector-meson form factors to the lack of rotational covariance in relativistic quantum mechanical models. The uncertainties in the vector-meson form factors associated with this sensitivity become significant above  $q^2 = 1 \text{ GeV}^2$  [5]. In contrast to this, the framework employed herein is fully covariant.

#### IV. SUMMARY

The electromagnetic form factors, associated moments and charge radii have been calculated for the  $\rho^+$ ,  $K^{*+}$ , and  $K^{*0}$  mesons within a Dyson-Schwinger based model using confined-quark propagators developed in phenomenological studies of  $\pi$ - and  $K$ -meson observables and vector-meson BS amplitudes that are closely related to the pseudoscalar amplitudes obtained from the same studies.

The calculated  $\rho$ -meson charge radius and electric-quadrupole moment are in excellent agreement with the values obtained from light-front quantum mechanical models, while the magnetic moment obtained herein is found to be 20% larger than the mean value obtained from quantum mechanical models.

The experimental difficulties that must be overcome to directly measure the vector-meson EM form factors will continue to limit our knowledge of these important observables in the future. However, indirect measurements of their static limits are possible and provide important information about quark dynamics and vector-meson bound states. In particular, the quadrupole moment provides an excellent probe of the mass scales in the quark propagator, while the charge radius principally probes the details of the vector-meson BS amplitude. Information about infrared observables provides constraints on and guidance for the construction of realistic models of the strong interaction as well as a test of our understanding of nonperturbative QCD.

#### ACKNOWLEDGMENTS

The authors acknowledge useful conversations with S.C. Capstick, J. Piekarewicz, and C.D. Roberts. This work is supported by the U.S. Department of Energy under Contracts DE-AC05-84ER40150 and DE-FG05-92ER40750 and the Florida State University Supercomputer Computations Research Institute which is partially funded by the Department of Energy through Contract DE-FC05-85ER25000.

- 
- [1] C.J. Bebek, *et al.*, Phys. Rev. D **13**, 25 (1976); S.R. Amendiola, *et al.*, Nucl. Phys. B **277**, 168 (1986); S.R. Amendiola, *et al.*, Phys. Lett. B **178**, 435 (1986); E.B. Dally *et al.*, Phys. Rev. Lett. **45**, 232 (1980); F. Cardarelli *et al.*, Phys. Rev. D **53**, 6682 (1996).
  - [2] C.D. Roberts, Nucl. Phys. A **605**, 475 (1996).
  - [3] C.J. Burden, C.D. Roberts and M.J. Thomson, Phys. Lett. B **371**, 163 (1996).
  - [4] G. López Castro and G. Toledo Sánchez, Phys. Rev. D **56**, 4408 (1997).
  - [5] B.D. Keister, Phys. Rev. D **49**, 1500 (1994).
  - [6] J.P.B.C de Melo and T. Frederico, Phys. Rev. C **55**, 2043 (1997).
  - [7] M.B. Hecht and B.H.J. McKellar, Phys. Rev. C **57**, 2638 (1998).
  - [8] M.A. Pichowsky and T.-S.H. Lee, Phys. Rev. D **56**, 1644 (1997).
  - [9] K.L. Mitchell and P.C. Tandy, Phys. Rev. C **55**, 1477 (1997).
  - [10] P. Maris and C.D. Roberts, Phys. Rev. C **56**, 3369 (1997); P. Maris, C.D. Roberts and P.C. Tandy, Phys. Lett. B **420**, 267 (1998).
  - [11] M.R. Frank and C.D. Roberts, Phys. Rev. C **53**, 390 (1996).
  - [12] A. Bashir and M.R. Pennington, Phys. Rev. D **50**, 7679 (1994).
  - [13] J.S. Ball and T.-W. Chiu, Phys. Rev. D **22**, 2542 (1980).
  - [14] F.T. Hawes, C.D. Roberts and A.G. Williams, Phys. Rev. D **49**, 4683 (1994); F.T. Hawes, A.G. Williams and C.D. Roberts, Phys. Rev. D **51**, 3081 (1995).
  - [15] R.G. Arnold, C.E. Carlson and F. Gross, Phys. Rev. C **21**, 1426 (1980).
  - [16] P. Maris and C.D. Roberts, *Pseudovector components of the pion,  $\pi^0 \rightarrow \gamma\gamma$ , and  $F_\pi(q^2)$* , LANL e-print # nucl-th/9804062, (1998).
  - [17] P. Geiger and E.S. Swanson, Phys. Rev. D **50**, 6855 (1994).
  - [18] P.C. Tandy, Prog. Part. Nucl. Phys. **39**, 117 (1997).
  - [19] R. Alkofer, A. Bender and C.D. Roberts, Int. J. Mod. Phys. A **10**, **23** (1995) 3319.
  - [20] Yu. Kalinovskiy, K.L. Mitchell, and C.D. Roberts, Phys. Lett. B **399**, 22 (1997).
  - [21] The “diffractive radius” of the  $\rho$  meson is given by:  $r_\rho^2 = 4b_{\rho N}(W) - 2b_{NN}(W) - 4\alpha_1 \ln(\alpha_1 W^2)$ , where  $W \geq 10 \text{ GeV}$  is the CM energy,  $\alpha_1 = 0.25 \text{ GeV}^2$  is the slope of the Pomeron trajectory, and  $b_{\rho N}$  and  $b_{NN}$  are the slopes of the differential cross sections at  $t = 0$  for  $\rho$ -meson electroproduction on a nucleon and nucleon-nucleon scattering, respectively. This result relies on the presumed analogy between these exclusive, diffractive processes and absorptive scattering in quantum mechanics.
  - [22] M.R. Frank, K.L. Mitchell, C.D. Roberts and P.C. Tandy, Phys. Lett. B **359**, 17 (1995).